



# Modeling the Distribution of Mountain Permafrost in Chile

Alexander Brenning<sup>1,\*</sup>, Guillermo F. Azócar<sup>2,\*</sup>, Pablo Iribarren Anacona<sup>3</sup>, Kenji Yoshikawa<sup>4, 2</sup>, Gino Casassa<sup>5, 6</sup>, Pedro Straub-Bustamante<sup>2</sup>, Duilio Fonseca-Gallardo<sup>2</sup>, and Jorge Huenante<sup>7</sup>

**Correspondence:** Alexander Brenning (alexander.brenning@uni-jena.de) and Guillermo F. Azócar (gazocar@atacamamb.com)

Abstract. Mountain permafrost is an important feature affecting slope stability and hydrological processes, yet its distribution remains poorly understood in many parts of the world, including Chile. This study develops the first countrywide highresolution (30 m × 30 m) model of mountain permafrost distribution in mainland Chile, using geomorphological evidence from intact (active and inactive) and relict rock glaciers, along with empirical indicators of permafrost presence/absence primarily derived from borehole temperature records, test pits, and surface temperature measurements. We employ a generalized additive model representing local and regional trends by incorporating mean annual air temperature, potential incoming solar radiation, and latitude as predictors. This model achieved an area under the receiver operating characteristic curve (AUROC) of 0.70 (0.74) in spatial (non-spatial) cross-validation. The model's predictions generate a Permafrost Favorability Index (PFI), which expresses the potential of permafrost occurrence conditional on the predictor variables. Excluding glaciers, rock glaciers and vegetated surfaces, areas with PFI values  $\geq 0.75$  were classified as having favorable conditions for permafrost development. Under this criterion, approximately 1.06 % (8,042 km<sup>2</sup>) of mainland Chile exhibits conditions suitable for mountain permafrost, concentrated in the Atacama, Antofagasta, Coquimbo, and Santiago Metropolitan regions (21-32° S and 33-34° S). In contrast, permafrost is scarce or absent from the Maule to the Magallanes regions (south of ~36° S). The interpretation of PFI values should consider local environmental factors not included in the model, such as snow cover duration, clast size, soil properties, and surface albedo. These variables may influence the presence or absence of permafrost locally and should be accounted for using an interpretative guide. This first version of the permafrost distribution model provides a baseline for understanding its general distribution in Chile, which should be refined as new empirical evidence and improved subsurface temperature records become available in the future.

<sup>&</sup>lt;sup>1</sup>Friedrich Schiller University Jena, Department of Geography, Löbdergraben 32, 07743 Jena, Germany

<sup>&</sup>lt;sup>2</sup>Atacama Ambiente Consultores, Huechuraba, Región Metropolitana, Chile

<sup>&</sup>lt;sup>3</sup>Universidad Austral de Chile, Instituto de Ciencias de la Tierra, Valdivia, Chile

<sup>&</sup>lt;sup>4</sup>University of Alaska Fairbanks, Institute of Northern Engineering, Water and Environmental Research Center, Fairbanks, Alaska, USA

<sup>&</sup>lt;sup>5</sup>Universidad de Magallanes, Punta Arenas, Chile

<sup>&</sup>lt;sup>6</sup>Instituto Antártico Chileno, Punta Arenas, Chile

<sup>&</sup>lt;sup>7</sup>Dirección General de Aguas, Santiago, Chile

<sup>\*</sup>These authors contributed equally to this work.



30

40



#### 1 Introduction

Mountain permafrost is a key component of high-altitude environments, influencing slope stability (Harris et al., 2001; Huggel et al., 2010) and hydrological systems (Jones et al., 2019; Arenson et al., 2022). Its study is crucial not only for understanding the impacts of climate change on fragile mountain ecosystems but also for mitigating risks to human livelihoods and economic activities in these regions. In the Andes, mountain permafrost has gained growing attention as mining, water resource management, and infrastructure development increasingly expand into arid and semi-arid high-altitude areas (Brenning and Azócar, 2010a; Masiokas et al., 2020). There are currently no regulations that specifically address environmental impacts in permafrost areas, although political discussions have been ongoing since 2019 in the context of the proposed glacier protection legislation (Senate of Chile, 2023). Despite the significance of mountain permafrost, its spatial distribution remains poorly understood in the Andes due to limited empirical data and model-based assessments. This study addresses this gap by developing the first high-resolution permafrost favorability model in Chile.

Empirical models combining observational data with topographic and climatic predictor variables provide an effective means of approximating permafrost distribution at regional scales (Keller, 1992; Gruber and Hoelzle, 2001; Lewkowicz and Ednie, 2004; Janke, 2005; Boeckli et al., 2012a, b; Gruber, 2012; Sattler et al., 2016; Marcer et al., 2017; Azócar et al., 2017; Deluigi et al., 2017; Hu et al., 2024). While such models have been widely applied in many mountain regions, in the Andes, however, their application and therefore our knowledge of the spatial distribution of mountain permafrost is more limited. Previous studies covering the Andean region are either very general and based on coarse-resolution global climate models (Gruber, 2012; Saito et al., 2015), or they focus on specific region, such as the semi-arid Andes of central-northern Chile (Azócar et al., 2017).

Recent advances in gathering evidence of permafrost presence in this remote mountain region along with improved climate data (Brun et al., 2022) and better computer processing present a unique opportunity to model permafrost distribution at finer spatial resolutions and broader scales in the Andes. In addition to an increasing availability of geomorphological evidence (Dirección General de Aguas, 2022a, or Chilean Water Directorate, hereafter DGA), government-led monitoring programs and environmental baseline studies have become important sources of in-situ permafrost observations (Yoshikawa et al., 2025).

Rock glaciers, as geomorphological indicators, have become key proxies for mountain permafrost distribution due to their association with permafrost conditions (Janke, 2005; Boeckli et al., 2012a; Sattler et al., 2016; Azócar et al., 2017; Hu et al., 2024; Mahanta et al., 2024). Despite their abundance in the Andes, their use in permafrost modeling has been underexplored. A key challenge is that rock glaciers, due to their downslope movement and ice-rich content, can extend into permafrost-free terrain and exhibit delayed responses to climatic changes. Bias corrections, such as elevation offsets, are necessary to account for these effects (Boeckli et al., 2012a; Azócar et al., 2017; Cao et al., 2021).

This study, which is based on a project conducted for the DGA (2022a), delivers the first high-resolution ( $30\,\mathrm{m}\times30\,\mathrm{m}$ ) statistical model of permafrost distribution across mainland Chile, integrating geomorphological evidence (e.g., rock glacier activity status), field data (e.g., borehole and surface temperature records), and topoclimatic predictors (e.g., mean annual air temperature and potential incoming solar radiation). Empirical models, including generalized additive models (GAMs), were





used to capture nonlinear relationships between predictors and permafrost presence or absence. GAMs are particularly suitable for this purpose as they balance flexibility and interpretability (Hjort and Luoto, 2013; Goetz et al., 2015). Our model generates a regionalization, conceptualized as a Permafrost Favorability Index (PFI), that reflects the likelihood of permafrost occurrence conditional on the available environmental predictors (Boeckli et al., 2012a; Azócar et al., 2017). The results are compared to the global permafrost zonation index of Gruber (2012).

This research provides a baseline assessment of the potential spatial distribution of mountain permafrost under current climatic conditions in Chile. By combining landform-based and field-observed evidence, it establishes a foundation for future investigations into permafrost characteristics, dynamics, and sensitivity to climate change. The findings also address critical knowledge gaps in the Andean cryosphere and offer a platform for future studies.

### 2 Study area

The study area spans the entire length of mainland Chile located in South America, encompassing the Andes mountain range from approximately  $18^{\circ}$  S in the north to  $56^{\circ}$  S in the south. This region covers diverse climatic and topographic conditions, ranging from the hyper-arid Atacama Desert in the north to the cool temperate zone in the south, with tenfold differences in annual precipitation. Peak elevations frequently exceed  $5{,}000\,\mathrm{m}$  a.s.l. in the northern and central Andes, occasionally even  $6{,}000\,\mathrm{m}$ , as at Nevado Ojos del Salado  $(6{,}893\,\mathrm{m}$  a.s.l.,  $27^{\circ}$  07′ S) or Volcán Tupungato  $(6{,}570\,\mathrm{m}$  a.s.l.,  $33^{\circ}$  21′ S), and gradually declining toward the southern Andes with summit elevations rarely above  $3{,}000\,\mathrm{m}$  a.s.l. (e.g., Monte San Lorenzo,  $3{,}706\,\mathrm{m}$  a.s.l.,  $47^{\circ}$  35′ S).

The 0° C isotherm altitude (Zero Isotherm Altitud, ZIA), a key control on permafrost distribution, declines gradually with increasing latitude. In the northern Chilean Andes, it is located around 4,500–5,000 m a.s.l., decreasing to ~1,000 m in the southernmost part of the study area (Masiokas et al., 2020).

Vegetation is sparse at high elevations, particularly in the arid and semi-arid Andes north of  $\sim 34^{\circ}$  S, with the exception of azonal wetlands and floodplains. Toward the south, alpine vegetation only becomes more prevalant —and summit elevations high enough— at elevations close to the ZIA south of  $\sim 41^{\circ}$  S. Nevertheless, the treeline is also much lower (e.g., at  $\sim 1,200$  m a.s.l. at  $\sim 41^{\circ}$  S and  $\sim 600-700$  m at  $\sim 54^{\circ}$  S; Daniels and Veblen, 2003; Hansson et al., 2023) and therefore remains at a significant altitudinal distance to possible permafrost occurrences.

The distribution of glaciers, rock glaciers, and permafrost reflects these latitudinal gradients in climate and topography. In the north to central Chilean Andes, summit elevations exceed the modern equilibrium line altitude (ELA), typically above 5,000 m a.s.l. north of 31° S (Azócar and Brenning, 2010; Masiokas et al., 2020). Nevertheless, glaciers in the northern Chilean Andes are scarce and often limited to small glacierets or perennial snow patches. In the southern Andes, the ELA descends to altitudes below 1,500 m a.s.l. due to increased precipitation and cooler temperatures, facilitating the development of extensive ice fields such as the Northern and Southern Patagonian Ice Fields (Masiokas et al., 2020).

Rock glaciers, as permafrost landforms, are distributed across the Andes but exhibit distinct latitudinal and altitudinal patterns that are more closely related to the ZIA than to the ELA of glaciers. Active and inactive rock glaciers are prevalent





above  $4,200\,\mathrm{m}$  a.s.l. in the arid and semi-arid northern Andes. In central Chile, active rock glaciers are observed mainly above  $3,500\,\mathrm{m}$  a.s.l., whereas in southern Chile, their presence diminishes due to higher precipitation and the absence of suitable debris accumulation. There are gaps in the distribution of rock glaciers in northern Chile between  $24^{\circ}\,\mathrm{S}$  and  $26^{\circ}\,\mathrm{S}$ , and in southern Chile from  $36.5^{\circ}\,\mathrm{S}$  to  $43.5^{\circ}\,\mathrm{S}$ .

### 90 3 Methods and data

This section outlines the data sources and statistical methods used to model permafrost distribution across mainland Chile. We detail the response variable based on geomorphological and in-situ evidence, the derivation of key predictor variables such as MAAT (mean annual air temperature) and PISR (potential incoming solar radation), and the application of a GAM to produce a high-resolution permafrost favorability index.

# 5 3.1 Response and predictor variables

#### 3.1.1 Permafrost evidence

The response variable for modeling permafrost distribution was derived from an inventory of geomorphological and empirical evidence of permafrost presence and absence across mainland Chile. Two main sources of data were used: (1) a comprehensive rock glacier inventory and (2) in-situ evidence from boreholes, test pits, and ground surface temperature measurements.

## 100 Rock glacier inventory

Rock glaciers, geomorphological indicators of permafrost, were identified and classified based on their distinct morphological features, such as tongue- or lobe-shaped forms with surface ridges and furrows indicative of deformation (Barsch, 1996; Roer and Nyenhuis, 2007). Active and inactive rock glaciers, grouped together as intact forms, were distinguished from relict forms using criteria adapted to the conditions in the Andes (Azócar et al., 2017). While intact rock glaciers are often characterized by steep fronts and unstable rocks, relict forms exhibit collapsed surfaces indicative of ice loss. Given the inherent subjectivity in interpreting these features from satellite imagery, intact forms were treated as a single category.

Rock glacier data were compiled from (1) the Public Glacier Inventory (PGI) of the DGA (2022b) containing only intact rock glaciers, (2) an existing inventory for the Huasco to Choapa catchments in north–central Chile (Azócar et al., 2017), and additional relict landforms mapped manually across the Andes for this study. Rock glaciers were represented by point features marking their root zones, with the exception of the inventory data from (Azócar et al., 2017), which represented toe locations that were bias-adjusted in the modeling process (see Sect. 3.2). Root-zone points were extracted from the PGI polygon data using an automated extraction procedure.

The activity status of all rock glaciers was assessed based on visual interpretation of ESRI World Imagery (resolution  $< 1\,\mathrm{m}$ ) following a criteria catalog developed for this study based on previous studies (Table 1) (Barsch, 1996; Burger et al., 1999; Roer and Nyenhuis, 2007; Azócar et al., 2017). In the case of status information included in existing inventories, the classification was re-assessed.





**Table 1.** Evaluation of geomorphological, geomorphometric, and environmental parameters for determining the dynamics of rock glaciers (RG) in the dry Andes.

Method / Indicator	Determined by	Data type	Suitability as an indicator for differentiating rock glaciers		
			Active vs. inactive	Inactive vs. relict	Active vs. relict
Slope angle of RG front	Steep / Smooth slope angle	Quantitative	Not suitable	Poor	Good
Geomorphological appearance of RG front	Indicative microforms of movement	Descriptive	Very good	Poor	Very good
Tone of the front in photographs and satellite images	Presence of a light tone	Descriptive	Very good	Good	Very good
Abundance of lichens or vegetation	Spatial distribution	Descriptive	Not suitable	Not suitable	Not suitable
Geomorphological appearance of the surface	Development of ridges and furrows	Descriptive	Poor	Poor	Good
Appearance of rocks on the RG surface	Weathering state and rock position	Descriptive	Poor <sup>1</sup>	Good <sup>1</sup>	Very good <sup>1</sup>
Stability of large rocks	Rock displacement	Descriptive	Poor <sup>2</sup>	Good <sup>2</sup>	Very good <sup>2</sup>
Occurrence of ice outcrops	Location and size of the outcrops	Descriptive	Not suitable <sup>3</sup>	Very good <sup>3</sup>	Very good <sup>3</sup>
Occurrence of active thermokarst	Locational characteristics	Descriptive	Not suitable <sup>4</sup>	Very good <sup>4</sup>	Very good <sup>4</sup>
Basal temperature of snow (BTS)	Beneath a snow cover > 0.8 m	Quantitative	Not suitable <sup>5</sup>	Good <sup>5</sup>	Good <sup>5</sup>
Dynamics measurements	GPS surveys	Quantitative	Good	Very good	Very good
Patches of perennial or persistent snow	Locational characteristics	Descriptive	Not suitable <sup>6</sup>	Not suitable / Very good <sup>6</sup>	Not suitable / Very good <sup>6</sup>
Water temperature from RG	Temperature measurements	Quantitative	Not suitable <sup>7</sup>	$Good^7$	$Good^7$

<sup>&</sup>lt;sup>1</sup> Generally, active and inactive RGs tend to have fresh rock fragments, often with overturned rocks. In contrast, relict RGs exhibit weathered rock fragments, sometimes covered with lichens. 2 On active and inactive RGs, large blocks can often be slightly displaced by human force, unlike in relict RGs where the rocks have settled and are much harder to move. 3 The occurrence of ice outcrops indicates a non-relict state but does not distinguish between active and inactive rock glaciers. Conversely, the absence of ice outcrops does not indicate the dynamic state of the RG. 4 The absence of active thermokarst does not necessarily indicate that the RG is active or inactive; however, the presence of active thermokarst could indicate that the RG is active or inactive but not relict. 5 BTS (basal temperature of snow) values  $> -2^{\circ}$  C indicate no permafrost, while BTS  $< -3^{\circ}$  C indicates a probable presence of permafrost. Therefore, measuring the basal snow temperature could be a useful indicator to differentiate between intact and relict RGs. However, the temperature thresholds defining the presence or absence of permafrost must be calibrated locally (see Lewkowicz and Ednie, 2004). <sup>6</sup> The absence of perennial snow patches does not necessarily indicate the absence of permafrost and, therefore, the activity level of a RG. However, the presence of perennial snow patches could be used as an indicator of the presence of permafrost and, consequently, active or inactive RGs (Haeberli, 1975). A temperature close to 0° C implies that water has permafrost contact within the RG; therefore, it would indicate an active or inactive RG state. However, a higher temperature does not necessarily mean there is no ice within a RG (Haeberli, 1975).

### In-situ evidence of permafrost

Complementing the rock glacier inventory, an extensive dataset of 238 in-situ observations was compiled to document the presence or absence of permafrost (DGA, 2022a). These data, primarily sourced from government and mining-related studies, include test pits (TP; 135 point observations of subsurface conditions), ground surface temperature (GST; 22 locations), and boreholes (BH; 81 ground temperature records; 12 of the BH are also documented in a recent study by Koenig et al. 2025). Evidence was classified based on the likelihood of permafrost presence or absence, using established thresholds and expert validation. Of the total observations, 93 indicated permafrost presence (3 confirmed, 36 probable, and 54 possible), while 145 indicated absence (16 confirmed, 129 uncertain). The majority of these observations are located in the Atacama region (181 between 26° S and 28° S), while only isolated observations exist south of the Metropolitan Region and the southern Magallanes Region (6 south of 34° S; see Fig. 1).





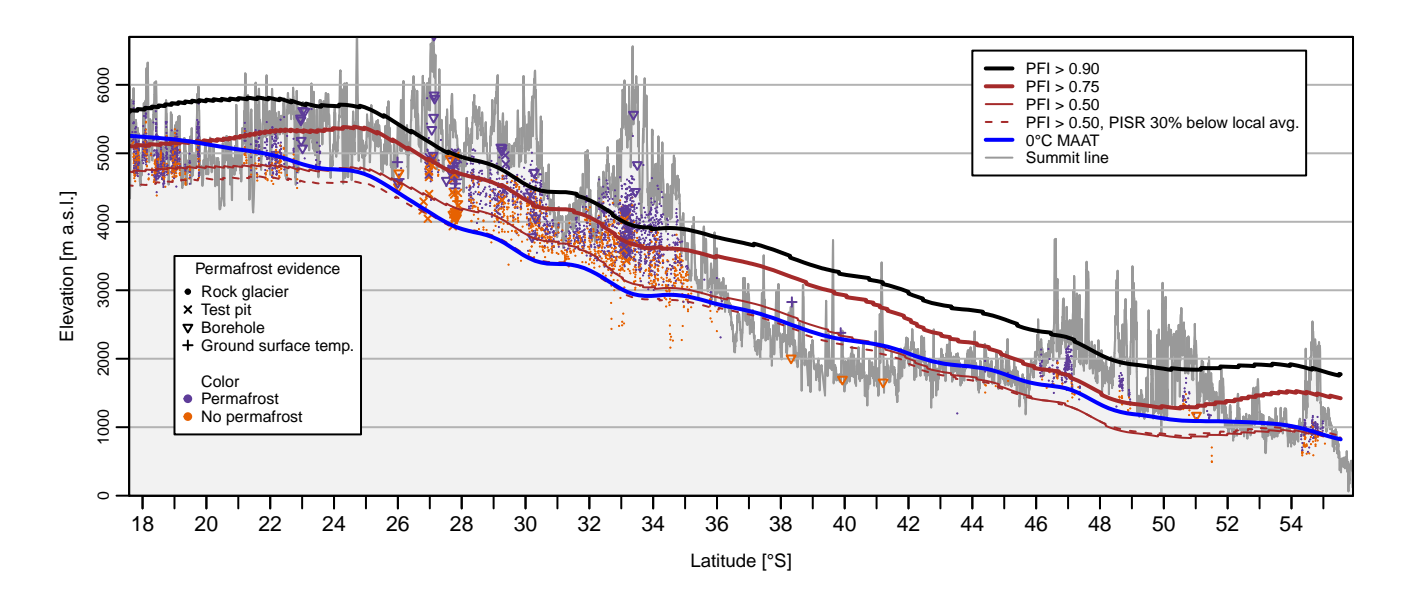


**Figure 1.** Latitudinal shift in the altitudinal distribution of PFI in mainland Chile: Elevation at which the PFI has values 0.90, 0.75 and 0.50 at PISR equal to the regional mean, and for a PFI of 0.75 and PISR 30 percent below regional mean. The  $0^{\circ}$  C isotherm altitude and permafrost evidences are shown for reference. Latitudes of in-situ evidences were perturbed to reduce clutter, and only a random sample of evidences is shown where density is highest (in-situ evidences:  $27-29^{\circ}$  S; rock glaciers:  $27-36^{\circ}$  S).

# 3.1.2 Predictor variables

130

135

140

The predictor variables used in the permafrost distribution model included topoclimatic and topographic data, specifically MAAT, PISR, and latitude, all of which were derived at or resampled to a  $30\,\mathrm{m}\times30\,\mathrm{m}$  target resolution. As digital elevation model (DEM) we use the NASADEM product (NASA JPL, 2020), which provides full, gap-filled coverage of Chile's topography at this resolution.

MAAT was derived from CHELSA–BIOCLIM+ gridded climate datasets (Brun et al., 2022), which provide global temperature data (1979–2019 mean) at ~1 km  $\times$  1 km resolution. The dataset was resampled to  $30 \, \mathrm{m} \times 30 \, \mathrm{m}$  resolution using a GAM with NASADEM elevation and latitude as predictors. This model setup adjusts CHELSA–BIOCLIM+ data, allowing for a latitudinal temperature shift as well as latitudinally varying lapse rates. The final model used 27.6 effective degrees of freedom and achieved an  $R_{adj}^2$  of 0.893 with a residual standard deviation of 1.09° C and used a constant lapse rate of 0.005398° C m<sup>-1</sup>.

Potential Incoming Solar Radiation (PISR) represents the annual sum of direct and diffuse solar radiation and was calculated using SAGA GIS (v9.0.2; Conrad et al., 2015) based on the NASADEM. Annual PISR was estimated for clear-sky conditions in 30-minute time steps and at 10-day intervals, accounting for topographic shading. Regional atmospheric transmittance values were adjusted by latitude, ranging from 50% in northern Chile to 70% in southern regions with increased atmospheric moisture content. To improve model interpretability, PISR values were centered around the dataset's mean, creating a normalized





variable (CPISR) for input into the statistical model. A CPISR value of 1.2, for example, means that a location has a PISR 20% above the study area's mean value.

Additionally, latitude was used as a proxy for large-scale climatic gradients, especially those related to snow cover and precipitation characteristics.

#### 3.2 Statistical model

A GAM was implemented to predict the spatial distribution of permafrost in mainland Chile. GAMs extend generalized linear models (GLMs) by allowing nonlinear relationships between predictors and the response variable through the use of smoothing functions (Wood, 2017). They have been applied successfully to model rock glacier and mountain permafrost distribution as well as other geomorphological processes and landforms (Brenning and Azócar, 2010b; Hjort and Luoto, 2013; Brenning et al., 2015; Azócar et al., 2017). While the use of more flexible models such as random forests has been proposed in the context of permafrost modeling (Deluigi et al., 2017; Hu et al., 2024; Mahanta et al., 2024), increases in model performance are often negligible or due to overfitting and may not outweigh the loss of interpretability compared to additive models (Goetz et al., 2015; Jiang et al., 2024).

As response variable Y we use an indicator variable of presence (Y=1) versus absence (Y=0) of (inferred or observed) permafrost conditions, which is modeled by means of a logistic link function. Our predictors are MAAT, CPISR, and latitude. The model can therefore be expressed as

$$\ln\left(\frac{P(\mathbf{x})}{1 - P(\mathbf{x})}\right) = \beta_0 + f_{\text{MAAT}}(\text{MAAT}(\mathbf{x})) + f_{\text{CPISR}}(\text{CPISR}(\mathbf{x})) + f_{\text{LAT}}(\text{LAT}(\mathbf{x})),$$
(1)

where  $P(\mathbf{x})$  is the probability of permafrost presence at location  $\mathbf{x}$ ,  $\beta_0$  is the intercept, and  $f_{\text{MAAT}}$ ,  $f_{\text{CPISR}}$ ,  $f_{\text{LAT}}$  are nonlinear smoothing functions for MAAT, CPISR, and latitude, respectively. We impose monotonicity constraints (Pya and Wood, 2015) to avoid overfitting and improve geomorphological plausibility by ensuring a monotonic decrease in predicted probabilities for increasing MAAT, CPISR, and latitude. In addition, model adjustments as outlined below are implemented to reduce possible biases.

Model predictions at the probability scale are used as to define a permafrost favorability index (PFI) that highlights areas with potential permafrost conditions (Boeckli et al., 2012a; Azócar et al., 2017).

The model was fitted in R using the scam package, which extends the mgcv implementation of spline-based GAMs (Wood, 2017; Pya, 2023) for model fitting, RSAGA and terra for spatial data processing (Brenning et al., 2022; Hijmans, 2025), and sperrorest for model assessment (Brenning, 2012). Predictor variables were extracted and processed using SAGA GIS (v9.0.2; Conrad et al., 2015).

# Model assessment

170

Model performance was evaluated using spatial cross-validation (CV) to account for spatial dependencies in the data and assess how well the model generalizes from the data (Brenning, 2012; Jiang et al., 2024). We used leave-one-block-out CV with k = 10 blocks created by k-means clustering. The area under the receiver operating characteristic curve (AUROC) was



180

185

190



calculated as a goodness-of-fit measure. AUROC values range from 0.5 (no predictive power) to 1.0 (perfect separation of both classes), with values above 0.70 considered acceptable (Hosmer and Lemeshow, 2000).

# Model adjustments

To refine the permafrost distribution model and address potential biases, several adjustments were implemented, including the use of altitudinal offsets, the exclusion of certain surface types, and the definition of a model domain based on climatic thresholds. Such adjustments have been implemented previously in similar studies (Boeckli et al., 2012a; Azócar et al., 2017).

While intact rock glaciers (active and inactive) are considered indicators of the lower limit of permafrost, their distal parts have often advanced into zones where climatic conditions are less favorable for permafrost. To account for this, the model considered the root zones (maximum altitude) of rock glaciers as more representative of conditions favorable for permafrost preservation, rather than their toes. For rock glaciers in the Huasco, Elqui, Limarí, and Choapa basins, an altitudinal offset of 89 m, estimated by Azócar et al. (2017), was therefore applied as an adjustment, while in the other areas, actual root-zone locations were available.

To align with the project scope, we constrained the model domain using exclusion criteria related to glaciers, vegetation, and MAAT. Glacier-covered areas were removed as glaciers in this region cannot be assumed to be cold-based. Glacier polygons were sourced from the PGI (DGA, 2022b). Similarly, areas with significant vegetation cover were excluded using a normalized difference vegetation index (NDVI) derived from Landsat imagery (2013–2022; U.S. Geological Survey Landsat 8 Collection 1 Tier 1 32-Day NDVI Composite). A threshold of  $\geq 0.2$  was applied to the 75th percentile of NDVI during this period to generate a binary mask of vegetated zones. Thus, even sparse vegetation with a short greening period is masked out. Areas with MAAT above  $5^{\circ}$  C were also discarded.

# 4 Results

# 4.1 Exploratory analysis

The dataset for modeling permafrost distribution consisted of 10,517 observations, including 6,187 intact and 4,092 relict rock glaciers from multiple inventories, and in-situ evidence (DGA, 2022a). Observations were classified into two categories: presence of permafrost (6,279 observations) and absence of permafrost (4,238 observations).

MAAT, CPISR and latitude each were negatively associated with permafrost presence (univariate AUROC values: 0.61, 0.62 and 0.52, respectively; Table 2). Pairwise Pearson and Spearman correlations of predictors were weak (absolute values below 0.40), indicating no concurvity issues.

# 4.2 Model performance and interpretation

In the model of permafrost presence versus absence, all predictor variables (MAAT, CPISR, and latitude) showed a significant association with the response (p-values < 0.001; Table 2), using moderately nonlinear smoothing functions with between 3.0 and 4.9 effective degrees of freedom for each predictor (Fig. 2). The monotonicity constraint on latitude eliminated an





**Table 2.** Summary statistics of the permafrost distribution model, a shape-constrained GAM, and its predictor variables (edf: effective degrees of freedom).

Predictor	AUROC	edf	p-value	Odds ratio for selected contrast
MAAT	0.61	4.90	< 0.001	2.1 for −2 K contrast
CPISR	0.62	4.40	< 0.001	2.5  for  -0.2  contrast
Latitude	0.52	3.01	< 0.001	$\approx 7.0$ in extreme north vs. center
				$\approx 0.34$ in extreme south vs. center

implausible overshoot or 'cold anomaly' in a data-poor region in south-central Chile (37–44° S), which would have been modeled with 4.9 additional degrees of freedom if an unconstrained model had been used. Using spatial CV, the model's AUROC showed 'acceptable' discrimination between presence and absence of permafrost, with a mean AUROC of 0.74 for random partitions and 0.70 for spatial blocks. This difference suggests that the model generalizes well from the data.

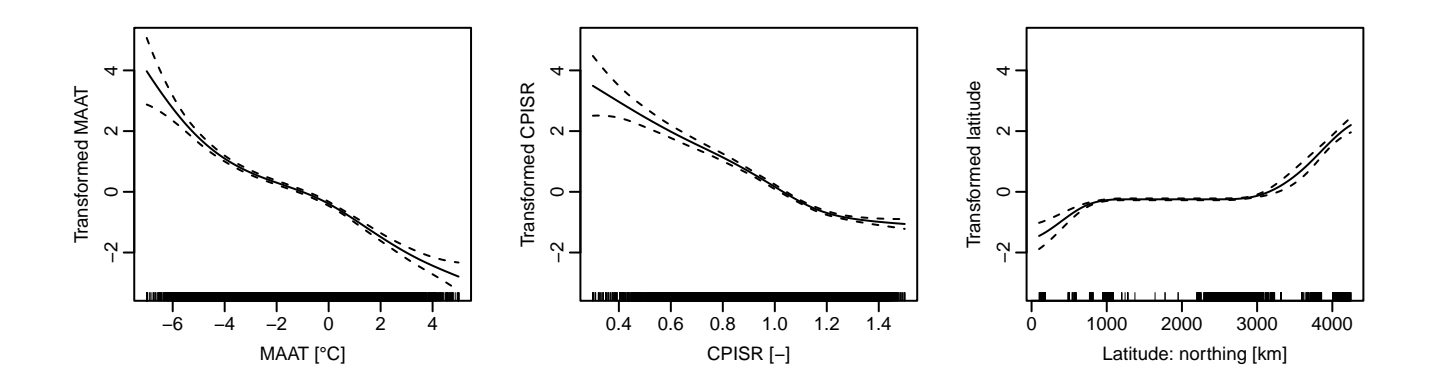


Figure 2. Nonlinear transformation functions of the shape-constrained GAM of permafrost distribution in mainland Chile. Transformed values on the y axes are on the logit scale.

In the interpretation of predictor–response relationships, the odds of permafrost presence were found to be about 2.1 times higher for a 2 K lower MAAT, when focusing on the  $-4^{\circ}$  C to  $0^{\circ}$  C range. A CPISR difference of 0.2 was associated with an odds ratio of 2.5, when accounting for the other variables in the model. Latitudinally, the model predicted increased permafrost presence in the northernmost part (odds ratio up to 7.0 compared to central Chile) and decreased odds in the extreme south (odds ratio as low as 0.34), indicating more favorable and unfavorable conditions, respectively, than in central Chile, under otherwise equal conditions.



220

230



# 4.3 Field validation and interpretation of PFI

The PFI was validated against local borehole data, the most reliable, though non-randomly distributed evidence for permafrost presence or absence. Of 80 borehole sites, 35 indicated permafrost presence, and 45 indicated absence. Model performance was evaluated using confusion matrices with varying PFI thresholds (0.75, 0.85, and 0.90). At a threshold of PFI  $\geq$  0.75), the model achieved high specificity (96%), correctly predicting almost all sites without permafrost, but only 40% sensitivity, or permafrost detection rate (Table 3). Reducing the threshold to PFI  $\geq$  0.50 improved sensitivity to 83%, with a substantial decrease in specificity to 33%. In terms of the predictive value of identified permafrost areas, 88% (49%) of identified permafrost locations presented borehole evidence of permafrost, when applying a PFI threshold of 0.75 (0.50). Based on these results, a threshold of 0.75 was deemed appropriate for identifying conditions favorable for permafrost existence, while permafrost less likely to occur but still considered possible for PFIs between 0.50 and 0.75.

**Table 3.** Summary statistics of permafrost prediction accuracy on the training sample and for the borehole data (N=80) using PFI thresholds of 0.50 and 0.75.

	Entire	sample	Boreholes only		
Indicator	$\mathrm{PFI} \geq 0.75$	$\mathrm{PFI} \geq 0.50$	$\mathrm{PFI} \geq 0.75$	$\mathrm{PFI} \geq 0.50$	
Overall accuracy	0.59	0.68	0.71	0.55	
Sensitivity	0.37	0.80	0.40	0.83	
Specificity	0.91	0.50	0.96	0.33	
Positive predictive value	0.86	0.70	0.88	0.49	
Negative predictive value	0.49	0.63	0.67	0.71	

The local permafrost evidence clearly highlights that the global PZI is too restrictive in the Chilean Andes. Using a threshold of PZI  $\geq 0.50$ , only  $16\,\%$  of the all positive field evidences and  $37\,\%$  of the borehole-based permafrost evidences would be identified as potential permafrost locations, indicating a low sensitivity even with this relatively low threshold.

# 4.4 Distribution and interpretation of PFI

The predicted PFI's generalized lati-altitudinal distribution is summarized in Fig. 1, showing that the transition from relict to intact rock glaciers takes place mostly within a  $500 \,\mathrm{m}$  elevation band above the ZIA, or between about  $-3^{\circ} \,\mathrm{C}$  and  $0^{\circ} \,\mathrm{C}$  MAAT. In the southern part and especially in the extreme north, this transition occurs at somewhat higher MAAT, around  $0^{\circ} \,\mathrm{C}$  and even above, respectively. This transition band generally corresponds to the  $0.50\text{--}0.75 \,\mathrm{PFI}$  range. Nevertheless, favorable conditions can be shifted about  $500 \,\mathrm{m}$  downward where incoming solar radiation is low (dashed line in Fig. 1).

Assuming PFI ≥ 0.75 indicates conditions highly favorable for permafrost, approximately 1.06 % (8,042 km²) of mainland Chile may support permafrost, excluding glaciated and vegetated areas (Table 4). Considering that the PFI may not be reliable in exposed bedrock areas, which can be approximated by having slope angles 30° (Azócar et al., 2017), this reduces to 6,378 km².



240



**Table 4.** Potential distribution of mountain permafrost in mainland Chile by region: areas with PFI  $\geq 0.75$ .

Region	Surface area [km <sup>2</sup> ]	$PFI \ge 0.75 \text{ Area } [\text{km}^2]$	Share of region [%]
Mainland Chile	755,218	8,042	1.1
Arica and Parinacota	16,867	145	0.9
Tarapacá	42,285	108	0.3
Antofagasta	126,071	1,146	0.9
Atacama	75,661	3,283	4.3
Coquimbo	40,576	983	2.4
Valparaíso	16,323	335	2.1
Santiago Metropolitan Region	15,392	1,048	6.8
O'Higgins	16,349	287	1.8
Maule	30,321	16	0.1
Biobío	24,022	0.6	0.0
Ñuble	13,104	0.7	0.0
La Araucanía	31,838	0.3	0.0
Los Ríos	18,245	0.03	0.0
Los Lagos	48,408	2.0	0.0
Aysén	106,703	368	0.3
Magallanes and Chilean Antarctica <sup>1</sup>	133,053	320	0.2

<sup>&</sup>lt;sup>1</sup> Not including Antarctica.

Regions with the highest concentrations of favorable permafrost conditions are located in Atacama, Antofagasta, Coquimbo  $(21\text{--}32^{\circ}\,\mathrm{S})$ , and the Santiago Metropolitan Region  $(33\text{--}34^{\circ}\,\mathrm{S})$ , where extensive mountain areas exceed the critical elevation thresholds (Fig. 3). In contrast, regions south of Maule (~36° S) exhibit only isolated or no favorable conditions for permafrost due to higher temperatures and generally lower elevations. Statistics for the main catchments with likely permafrost presence are included in the Appendix in Table A1. This allows for a comparison with results of an earlier study in the semi-arid Andes (Huasco to Choapa basins), which obtained very similar estimates using a similar methodology  $(1,051\,\mathrm{km}^2)$  in Azócar et al. (2017) versus  $1,118\,\mathrm{km}^2$  in this study, both for PFI  $\geq 0.75$  and limited to slope  $<35^{\circ}$ ).

A qualitative interpretation guide was developed based on a similar document by Boeckli et al. (2012b) to aid governmental and public use of PFI maps (Fig. 4). In particular, the consideration of snow cover duration, surface material properties and climatic conditions are important for practical applications (see Sect. 5.1). Figure 5 shows a sample PFI map from central Chile, and additional maps are included in the Appendix (Fig. A1 and A2), highlighting specific high-altitude zones with the greatest potential for permafrost presence.





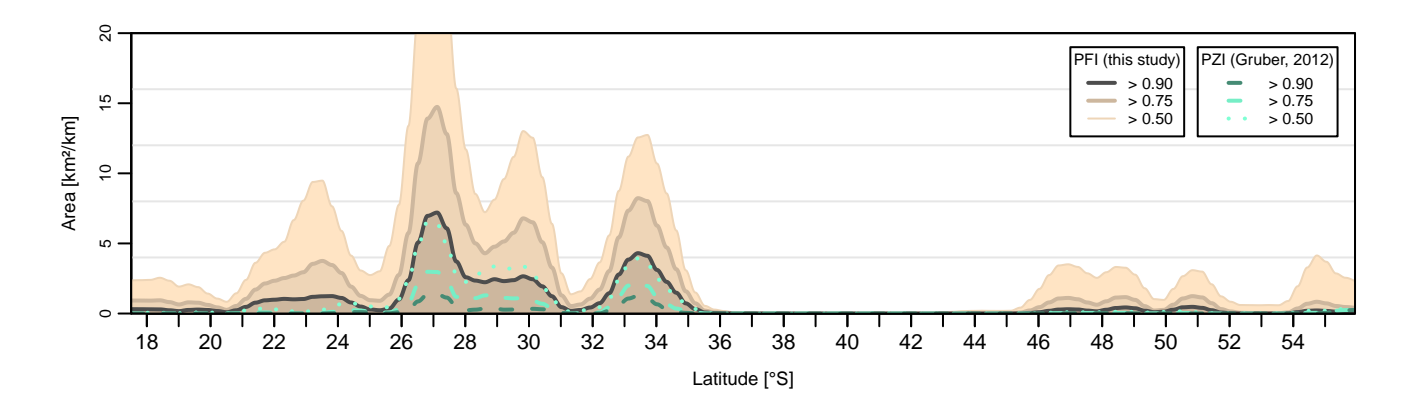


**Figure 3.** Latitudinal shift in the altitudinal distribution of PFI in mainland Chile: Area (in km<sup>2</sup> per 1 km north–south extent) with PFI greater than 0.90, 0.75, and 0.50. For comparison, the corresponding areas based on the PZI of Gruber (2012).

#### 5 Discussion

250

255

260

265

# 5.1 Rock glaciers and in-situ permafrost evidence

Rock glaciers are widely recognized as indicators of the lower limit of permafrost distribution, as evidenced by studies across various mountain regions globally (Boeckli et al., 2012a; Sattler et al., 2016; Azócar et al., 2017; Marcer et al., 2017; Baral et al., 2020; Mahanta et al., 2024). However, their use as a proxy for permafrost conditions requires bias adjustments and careful interpretation, particularly when considering local environmental variability (Boeckli et al., 2012a; Azócar et al., 2017; Cao et al., 2021). In this study, glaciers and areas with (even sparse) vegetation cover were excluded, although they may locally present permafrost. More importantly, only root-zone locations of rock glaciers were considered as permafrost evidence to exclude permafrost evidence from rock glacier tongues and lobes, which may have crept into non-permafrost terrain. Where only rock glacier toe locations were available, a bias adjustment was applied that accounts for the average altitudinal extent of rock glaciers (Azócar et al., 2017). Nevertheless, we point out that permafrost near the lower limit of its modeled potential distribution may be sporadic in extent and constituted of remnants that may not be preserved under present and future climatic conditions. Also, the classification of rock glacier activity status used in this study is subject to uncertainties and subjectivity, which can be reduced in the future by applying remote-sensing based criteria as proposed recently (RGIK Working Group, 2023; Cusicanqui et al., 2025; Rouyet et al., 2025).

The incorporation of additional in-situ permafrost evidence, including borehole measurements, enriches the empirical basis for model training and assessment. This is especially important in regions where rock glaciers are scarce or inexistent, as in parts of southern Chile or the most arid parts of the Atacama desert (Brenning, 2005; Yoshikawa et al., 2025). Future studies should prioritize expanding ground-truth observations across diverse environmental contexts, especially in non-rock glacier debris-covered terrain. Such studies would greatly benefit from targeted study designs rather than circumstantial evidence from various research or industrial activities.





# LEGEND OF THE PERMAFROST FAVORABILITY INDEX (PFI)

This map qualitatively represents the probability of permafrost occurrence in specific areas and under particular conditions. It is intended solely for practical interpretation by government entities and the general public. An isoline marking PFI values ≥ 0.75 is included as a reference for permafrost distribution.

#### LEGEND Permafrost Favorability Index (PFI)

 Permafrost present in all environmental conditions

0.75 Permafrost only present in col conditions and depending on

The interpretation of this legend should be supplemented by the interpretation guide, displayed to the right of this panel, which can be used locally to qualitatively refine the model's estimates.

More precise interpretations regarding the local presence of permafrost can also be inferred from the Permafrost Favorability Index (PFI) values produced by the model, which are available in raster format at a 30 m resolution.

It is important to note that more precise estimates of permafrost presence require local studies of permafrost distribution, including geophysical surveys, subsurface temperature monitoring in boreholes, and test pit excavations.

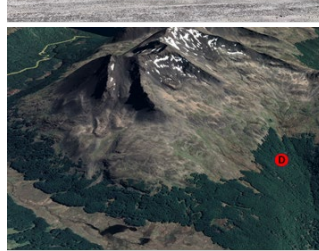
# LOCAL INTERPRETATION

# Clast size, soil properties, and vegetation:

A surface composed of openwork blocks, with no material filling the spaces between clasts, indicates cold conditions (A). In contrast, a coarse blocky surface layer with clasts embedded in accumulated finer material suggests warm conditions (B). Light-colored surfaces with high albedo may indicate cold conditions (C). Dense vegetation generally signifies the absence of permafrost (D).







## Rock Glaciers:

Active (intact) rock glaciers indicate the presence of permafrost within their underlying mass and surface area (E). However, it cannot be easily concluded that adjacent areas are favorable fo Fossil or relict rock glaciers indicate the absence of permafrost (F). In this study, areas covered by rock glaciers were excluded from the prediction domain, as they are part of the Public Glacier Inventory (IPG) managed by the Chilean Water Directorate (DGA).



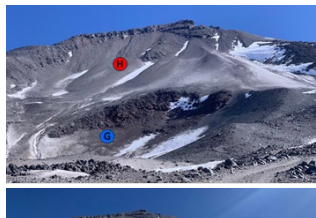


# Slope position and multi-year

snowfields

Thermal conditions along a slope vary due to the sorting of clasts, airflow within the slope, and snow redistribution. The base of a slope generally exhibits colder conditions (G), with coarse blocky material and snow accumulation due to avalanches.

avaranties. In contrast, the upper part of a slope tends to have warmer conditions due to smaller clasts and the presence of fine detritus between them (H). Fields of snow penitents or multi-year snowfields, which persist from one year to the next, may locally indicate colder conditions (I).





#### Rock walls

The thermal conditions of rock walls depend on their degree of fracturing. Highly fractured rock walls promote snow deposition and the infiltration of cold air (J), locally indicating colder conditions. Steep rock walls with flat, unfractured surfaces are more favorable for warmer conditions (K). This effect is more pronounced on sunexposed slopes compared to shaded areas.







Atacama Ambiente Consultores, A. Brenning

Figure 4. Legend and interpretation guide accompanying the permafrost favorability index map for mainland Chile. Original version in Spanish, by Atacama Ambiente Consultores; photos by K. Yoshikawa (A/B, C, H/G, I) and G. Azócar (E, J/K), perspective view (D) and satellite image (F) © Google Earth.

# 270 5.2 Model performance, interpretation, and future enhancements

The statistical performance of the model indicates that MAAT, CPISR, and latitude are significant predictors of permafrost distribution at the regional scale, consistent with previous studies (e.g., Brenning and Azócar, 2010b; Boeckli et al., 2012a).



275

280



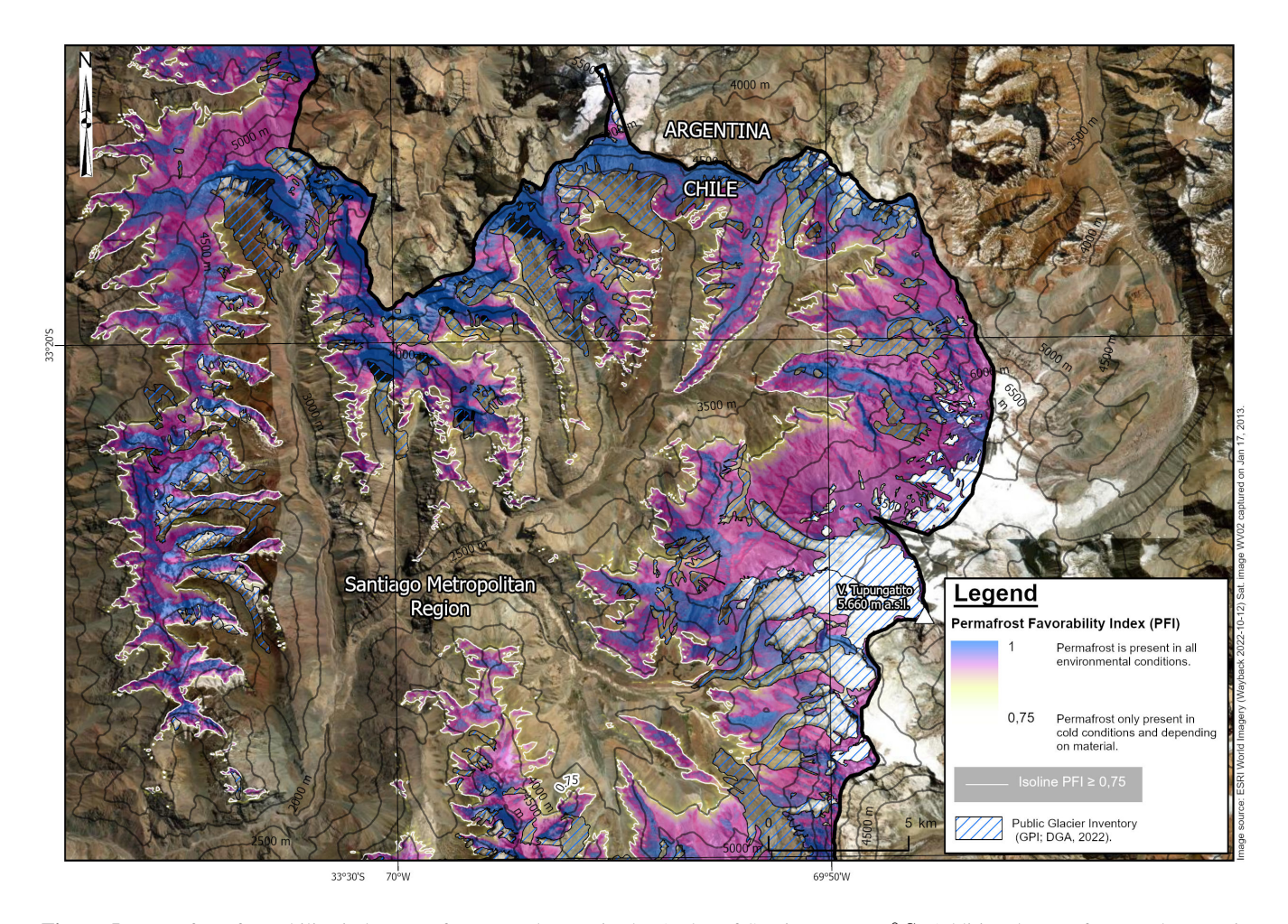


**Figure 5.** Permafrost favorability index map for a sample area in the Andes of Santiago at 33.3° S. Additional maps for sample areas in northern and southern Chile are included in the Appendix. Background satellite imagery from ESRI World Imagery Wayback (Wayback mosaic 04 September 2025, satellite image WV03 captured on 20 February 2023, https://livingatlas.arcgis.com/wayback/), last accessed 08 September 2025.

Our AUROC values (0.70 in spatial CV) are consistent with regional-scale permafrost modeling efforts in the Andes and Alps ( $\sim$ 0.75–0.80). Higher AUROC values in some studies ( $\geq$ 0.9) often result from more restrictive definitions of permafrost indicators, which reduce data heterogeneity but may artificially inflate model performance. This happens when inactive rock glaciers are excluded as indicators (Sattler et al., 2016; Marcer et al., 2017) or where low-elevation non-rock glacier areas are conceptualized as non-permafrost areas (Mahanta et al., 2024).

Although the model provides a useful regional-scale understanding of permafrost distribution, it does not fully account for critical local factors, such as snow redistribution by wind and avalanches or variations in soil and surface material properties. These factors are known to influence ground thermal regimes (Hoelzle et al., 2001; Boeckli et al., 2012a; Apaloo et al.,



290

295

300

305

310



2012; Koenig et al., 2025). For example, coarse blocky materials favor permafrost by enhancing ventilation and reducing heat retention, while fine-grained sediments tend to create warmer ground conditions (Gruber and Hoelzle, 2008; Pruessner et al., 2018; Wicky and Hauck, 2020). Apaloo et al. (2012) showed that in the Andes of Santiago (33.5° S), openwork boulder terrain was associated with  $\sim 0.6-0.8^{\circ}$  C lower mean annual ground surface temperatures (MAGST). Moreover, surfaces with 30 days of additional snow cover had a MAGST depression by  $0.1-0.6^{\circ}$  C. In the semi-arid Andes at  $30^{\circ}$  S, areas with long-lasting snow cover had a  $\sim 0.4^{\circ}$  C cooler MAGST (Centro de Estudios de Zonas Áridas, 2012).

The magnitude of these local modifications of ground thermal regimes highlights the importance of incorporating these effects in future modeling efforts. Field investigations of local-scale patterns of mountain permafrost outside of rock glaciers are now required to fill this gap, allowing future modeling efforts to combine regional-scale and local-scale patterns in order to reduce uncertainties. In addition to ground temperature monitoring, geophysical methods can play a crucial role in elucidating not only spatial patterns, but also characteristics such as ice content and thickness, which are of critical importance for the sensitivity of mountain permafrost to climate change (Hauck, 2013; Mollaret et al., 2019; Hilbich et al., 2022). Our model is instrumental in guiding future sampling and monitoring campaigns as it identifies areas with particularly high uncertainties, close to the proposed PFI thresholds.

In the meantime, the PFI offers a semi-quantitative rating of permafrost potential based on statistical relationships between predictors and observed permafrost evidence. As in similar modeling efforts (e.g., Boeckli et al., 2012a), the interpretation of PFI scores must consider the local environmental context as this is not incorporated in the current model in sufficient detail. We propose that PFI values greater than 0.9 should be interpreted as permafrost being very likely present regardless of specific local conditions. In PFI zones between 0.75 and 0.90, permafrost may be present primarily under cold local conditions (with shading or long-lasting snow cover) and dependent on surface materials. In areas with PFI values between 0.50 and 0.75, we conclude that permafrost presence is limited to favorable local conditions. In areas with lower PFI scores, permafrost should be expected to be absent in most circumstances.

# 5.3 Implications for regional permafrost distribution

The model predicts that more than  $8,000 \, \mathrm{km^2}$  of mainland Chile may have favorable conditions for permafrost occurrence (PFI  $\geq 0.75$ ). These areas are predominantly concentrated in high-altitude zones within the Atacama, Antofagasta, Coquimbo and Santiago Metropolitan regions, with minimal to no favorable conditions observed in southern regions (i.e., Maule to Magallanes). This pattern reflects the interplay between altitude, solar radiation, and latitude as first-order controls of permafrost occurrence. Being driven by local permafrost evidence, our model not only provides substantially more detail but also eliminates significant biases detected in the too restrictive global permafrost index, PZI (Gruber, 2012).

This research is the first to assess mountain permafrost distribution in southern Chile based on local geomorphological and in-situ evidence, significanctly extending earlier highly localized evidence from this large mountainous region (Selley et al., 2018). It furthermore refines previous models for central to northern Chile with new in-situ data from various sites and monitoring contexts, and it provides a generalized, synoptic vision across multiple rock glacier inventories.



315

320

330

335

340



This study also highlights the need for enhanced ground-truthing efforts to improve the calibration and validation of permafrost distribution models. A systematic approach to sampling ground temperatures across varied landforms and environmental conditions, coupled with expanded geophysical surveys, would strengthen the empirical foundation for future permafrost studies. At present, studies on local patterns are limited to near-surface ground temperatures (Apaloo et al., 2012; Centro de Estudios de Zonas Áridas, 2012), which provide limited insights into thermal conditions at relevant depths (Brenning et al., 2005). Additionally, the integration of remotely-sensed information with higher spatial and temporal resolution could refine the representation of local environmental factors, such as surface roughness, snow cover and vegetation dynamics (Jiang et al., 2020; Popescu et al., 2024), and confirm the activity status of rock glaciers (RGIK Working Group, 2023; Rouyet et al., 2025).

Although the PFI can suggest areas with cold ground conditions, it should not be used as a direct indicator of ground ice content. The presence of ground ice in permafrost may depend on local environmental conditions and the general climate setting (Hilbich et al., 2022).

# 325 6 Conclusions

This study presents the first high-resolution, regional-scale model of mountain permafrost distribution in Chile, providing a valuable foundation for understanding its potential spatial extent and first-order environmental controls. The model, based on geomorphological indicators, in-situ observations and topoclimatic variables, estimates that approximately 1.06% ( $8,042\,\mathrm{km^2}$ ) of mainland Chile may support permafrost, with favorable conditions concentrated in high-altitude areas of the Atacama, Antofagasta, Coquimbo and Santiago Metropolitan regions. In contrast, regions south of Maule exhibit limited permafrost due to lower elevations. Since the model does not account for local factors such as snow redistribution, substrate properties, and microclimatic effects, which can influence permafrost presence on finer spatial scales, it is important to keep these factors in mind when interpreting the proposed permafrost favorability index locally. In addition, ground ice presence and content should be expected to vary locally.

While rock glaciers are an established and relatively easy to classify proxy for permafrost distribution, their use introduces some biases that we account for through model adjustments and the use of and comparison to in-situ observations. Further ground-truthing, including borehole measurements and geophysical surveys, is essential to further refine the model and its bias adjustments in order to enhance model accuracy. Despite these limitations, the study contributes significantly to our knowledge about Chile's cryosphere and offers a valuable baseline for permafrost research and practical applications in infrastructure planning and geomorphological hazard assessments, and will serve as a starting point for future refinements and local adjustment.





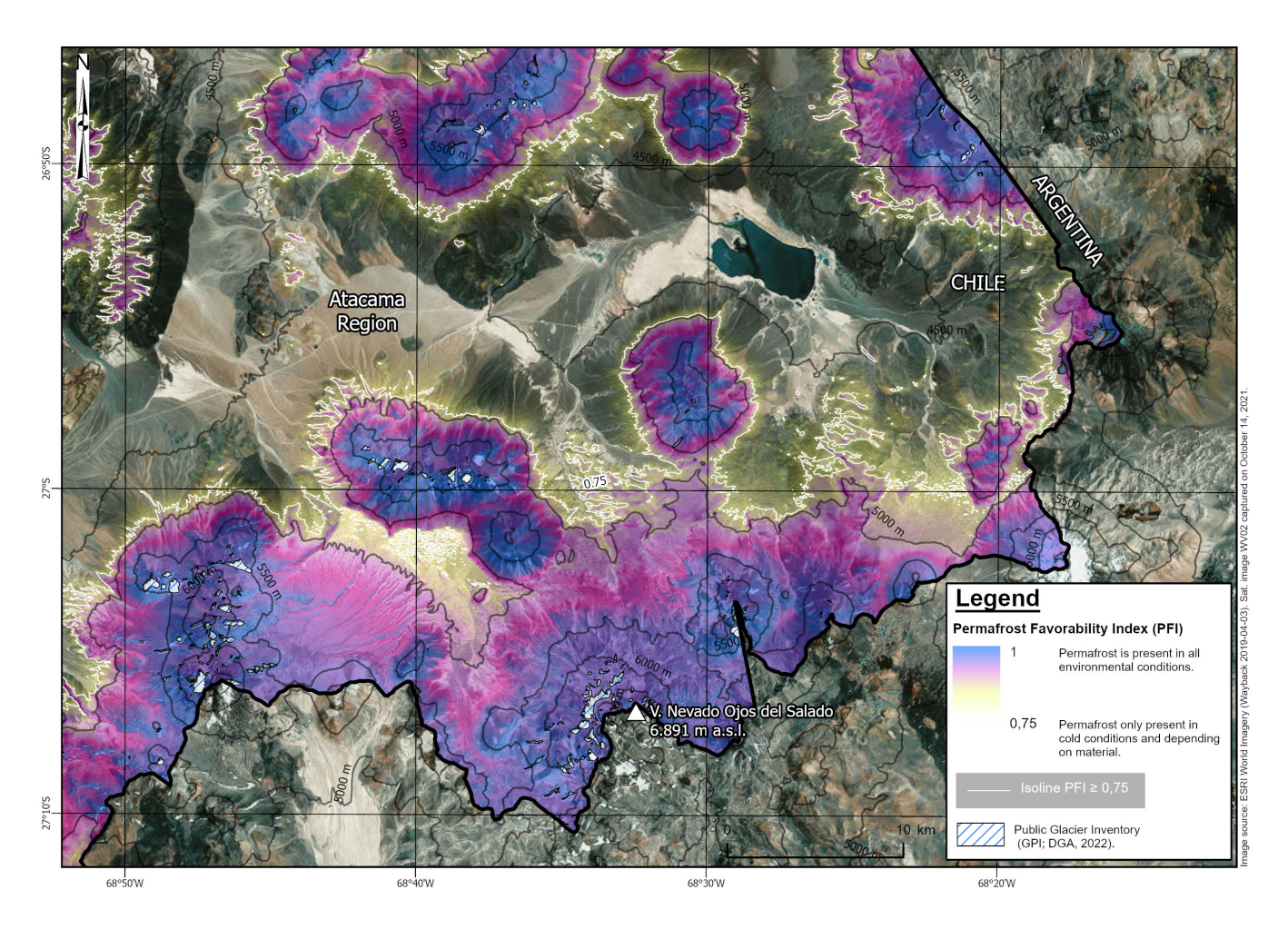


**Figure A1.** Permafrost favorability index map for a sample area in the dry Andes, Atacama region, at 27° S. Background satellite imagery from ESRI World Imagery Wayback (Wayback mosaic 12 December 2022, satellite image WV02 captured on 17 January 2013, https://livingatlas.arcgis.com/wayback/), last accessed 08 September 2025.







**Figure A2.** Permafrost favorability index map for a sample area in the Patagonian Andes, region of Magallanes and Chilean Antarctica, northeast of Cordillera Darwin at 54.4° S. Background satellite imagery from ESRI World Imagery Wayback (Wayback mosaic 13 April 2019, satellite image WV02 captured on 14 October 2021, https://livingatlas.arcgis.com/wayback/), last accessed 08 September 2025.





Table A1. Permafrost favorability index statistics by catchment, from north to south, for all river basins with more than  $50\,\mathrm{km}^2$  area of PFI  $\geq 0.75$ . Areas with PFI  $\geq 0.75$  and slope angle  $<35^\circ$  are shown to exclude likely bedrock areas. Catchment names are based on the official classification.

River basin	Area [km <sup>2</sup> ]	$\mathrm{PFI} \geq 0.75~\mathrm{[km^2]}$	Fraction [%]	PFI $\geq 0.75$ , slope $< 35^{\circ} \text{ [km}^2\text{]}$	Fraction [%]
Altiplano basins	11,368	168	1.5	143	1.3
Border catchments, Salar Michincha to Río Loa	2,675	89	3.3	81	3.0
Río Loa	33,081	222	0.7	194	0.6
Salar de Atacama	15,576	224	1.4	207	1.3
Border catchments, Salar Atacama to Socompa	4,055	124	3.1	120	3.0
Endorheic between Fronterizas and Salar Atacama	5,308	363	6.8	345	6.5
Endorheic Salar Atacama to Pacific slope	14,473	105	0.7	99	0.7
Endorheic between border and Pacific slope	15,618	2,197	14.1	2,163	13.9
Río Copiapó	18,703	617	3.3	552	3.0
Río Huasco	9,813	549	5.6	462	4.7
Río Elqui	9,825	645	6.6	530	5.4
Río Limarí	11,696	120	1.0	77	0.7
Río Choapa	7,653	75	1.0	49	0.6
Río Aconcagua	7,334	325	4.4	162	2.2
Río Maipo	15,273	1,038	6.8	572	3.7
Río Rapel	13,766	278	2.0	126	0.9
Río Baker	20,945	183	0.9	84	0.4
Río Pascua	7,590	145	1.9	80	1.1
Coastal, between Andrew Sound and eastern islands	17,829	158	0.9	80	0.4
Tierra del Fuego	42,219	86	0.2	42	0.1





Code and data availability. The permafrost index developed in this study is available through the digital repository of the Dirección General de Aguas (DGA) at https://snia.mop.gob.cl/PIA/handle/20.500.13000/126863.

Author contributions. GFA, AB, PIA, KY and GC contributed to the study conception and design. Material preparation and data collection were performed by GFA supported by PSB and DFG, and data analysis was conducted by GFA with support from AB. The first draft of the manuscript was written by AB based on a technical report mainly written by GFA and revised by GC, PIA, KY and AB, and all authors commented on previous versions of the manuscript. All authors read and approved the final manuscript.

Competing interests. Atacama Ambiente Consultores has received project funding from Dirección General de Aguas to conduct this research. The authors declare that they have no conflict of interest.

Acknowledgements. This publication is based on a project funded by the Dirección General de Aguas, Ministerio de Obras Públicas, Chile, under Grant 'Modelo de favorabilidad de ocurrencia de permafrost (PFI) en Chile Continental', S.I.T. No. 530, Ministerio de Obras Públicas, Chile, awarded to Atacama Ambiente Consultores (https://snia.mop.gob.cl/PIA/items/0df1c24d-f1ba-4afb-b250-615a40580d18).





#### References

- Apaloo, J., Brenning, A., and Bodin, X.: Interactions between seasonal snow cover, ground surface temperature and topography (Andes of Santiago, Chile), Permafrost and Periglacial Processes, 23, 277–291, https://doi.org/10.1002/ppp.1753, 2012.
  - Arenson, L. U., Harrington, J. S., Koenig, C. E. M., and Wainstein, P. A.: Mountain permafrost hydrology—A practical review following studies from the Andes, Geosciences, 12, 48, https://doi.org/10.3390/geosciences12020048, 2022.
- Azócar, G., Brenning, A., and Bodin, X.: Permafrost distribution modeling in the semi-arid Chilean Andes, The Cryosphere, 11, 877–890, https://doi.org/10.5194/tc-2016-100, 2017.
  - Azócar, G. F. and Brenning, A.: Hydrological and geomorphological significance of rock glaciers in the Dry Andes, Chile (27°–33°S), Permafrost and Periglacial Processes, 21, 42–53, https://doi.org/10.1002/ppp.669, 2010.
  - Baral, P., Haq, M. A., and Yaragal, S. B.: Assessment of rock glaciers and permafrost distribution in Uttarakhand, India, Permafrost and Periglacial Processes, 31, 31–56, https://doi.org/10.1002/ppp.2008, 2020.
- Barsch, D.: Rockglaciers: Indicators for the present and former geoecology in high mountain environments, Springer, Berlin, Germany, 1996.

  Boeckli, A., Brenning, A., Noetzli, J., and Gruber, S.: A statistical approach to modelling permafrost distribution in the European Alps or similar mountain ranges, The Cryosphere, 6, 125–140, https://doi.org/10.5194/tc-6-125-2012, 2012a.
  - Boeckli, L., Brenning, A., Gruber, S., and Noetzli, J.: Permafrost distribution in the European Alps: Calculation and evaluation of an index map and summary statistics, The Cryosphere, 6, 807–820, 2012b.
- Brenning, A.: Climatic and geomorphological controls of rock glacier in the Andes of central Chile, Ph.D. thesis, Humboldt-Universität zu Berlin, Mathematisch-Naturwissenschaftliche Fakultät II, Berlin, Germany, 2005.
  - Brenning, A.: Spatial cross-validation and bootstrap for the assessment of prediction rules in remote sensing: The R package 'sperrorest', in: IEEE International Symposium on Geoscience and Remote Sensing IGARSS, pp. 5372–5375, Munich, Germany, 2012.
  - Brenning, A. and Azócar, G. F.: Minería y glaciares rocosos: impactos ambientales, antecedentes políticos y legales, y perspectivas futuras, Revista de Geografía Norte Grande, pp. 143–158, https://doi.org/10.4067/S0718-34022010000300008, 2010a.
  - Brenning, A. and Azócar, G. F.: Statistical analysis of topographic and climatic controls and multispectral signatures of rock glaciers in the dry Andes, Chile (27°–33°S), Permafrost and Periglacial Processes, 21, 54–66, https://doi.org/10.1002/ppp.670, 2010b.
  - Brenning, A., Gruber, S., and Hoelzle, M.: Sampling and statistical analyses of BTS measurements, Permafrost and Periglacial Processes, 16, 383–393, https://doi.org/10.1002/ppp.541, 2005.
- Brenning, A., Schwinn, M., Ruiz-Páez, A. P., and Muenchow, J.: Landslide susceptibility near highways is increased by 1 order of magnitude in the Andes of southern Ecuador, Loja province, Natural Hazards and Earth System Sciences, 15, 45–57, https://doi.org/10.5194/nhess-15-45-2015, 2015.
  - Brenning, A., Bangs, D., and Becker, M.: RSAGA: SAGA geoprocessing and terrain analysis, https://CRAN.R-project.org/package=RSAGA, R package version 1.4.0, 2022.
- Brun, P., Zimmermann, N. E., Hari, C., Pellissier, L., and Dirk, N. K.: Global climate-related predictors at kilometer resolution for the past and future, Earth System Science Data, https://doi.org/10.5194/essd-2022-212, 2022.
  - Burger, K., Degenhardt, J., and Giardino, J.: Engineering geomorphology of rock glaciers, Geomorphology, 31, 93–132, 1999.
  - Cao, B., Li, X., Feng, M., and Zheng, D.: Quantifying overestimated permafrost extent driven by rock glacier inventory, Geophysical Research Letters, 48, e2021GL092 476, https://doi.org/10.1029/2021GL092476, 2021.





- 390 Centro de Estudios de Zonas Áridas: Caracterización y monitoreo de glaciares rocosos en la cuenca del río Elqui, y balance de masa del glaciar Tapado, Technical report, Dirección General de Aguas, Unidad de Glaciología y Nieves, Ministerio de Obras Públicas, Santiago, 2012.
  - Conrad, O., Bechtel, B., Bock, M., Dietrich, H., Fischer, E., Gerlitz, L., Wehberg, J., Wichmann, V., and Böhner, J.: System for Automated Geoscientific Analyses (SAGA) v. 2.1.4, Geosci. Model Dev., 8, 1991–2007, https://doi.org/10.5194/gmd-8-1991-2015, 2015.
- Cusicanqui, D., Lacroix, P., Bodin, X., Robson, B. A., Kääb, A., and MacDonell, S.: Detection and reconstruction of rock glacier kinematics over 24 years (2000–2024) from Landsat imagery, The Cryosphere, 19, 2559–2581, https://doi.org/10.5194/tc-19-2559-2025, 2025.
  - Daniels, L. D. and Veblen, T. T.: Altitudinal treelines of the southern Andes near 40°S, The Forestry Chronicle, 79, 237–241, https://doi.org/10.5558/tfc79237-2, 2003.
- Deluigi, N., Lambiel, C., and Kanevski, M.: Data-driven mapping of the potential mountain permafrost distribution, Science of The Total Environment, 590–591, 370–380, https://doi.org/10.1016/j.scitotenv.2017.02.041, 2017.
  - Dirección General de Aguas: Catastro de evidencias de permafrost en Chile, Technical Report S.I.T. No. 530, parte II de III, Ministerio de Obras Públicas, Chile, Santiago, Chile, prepared by Atacama Ambiente Consultores, 2022a.
  - Dirección General de Aguas: Metodología del inventario público de glaciares, Technical report, Ministerio de Obras Públicas, Chile, Santiago, Chile, 2022b.
- 405 Goetz, J., Brenning, A., Petschko, H., and Leopold, P.: Evaluating machine learning and statistical prediction techniques for landslide susceptibility modelling, Computers and Geosciences, 81, 1–11, 2015.
  - Gruber, S.: Derivation and analysis of a high-resolution estimate of global permafrost zonation, The Cryosphere, 6, 221–223, https://doi.org/10.5194/tc-6-221-2012, 2012.
- Gruber, S. and Hoelzle, M.: Statistical modelling of mountain permafrost distribution: Local calibration and incorporation of remotely sensed data, Permafrost and Periglacial Processes, 12, 69–77, https://doi.org/10.1002/ppp.374, 2001.
  - Gruber, S. and Hoelzle, M.: The cooling effect of coarse blocks revisited, in: 9th International Conference on Permafrost, edited by Kane, D. L. and Hinkel, K. M., vol. 1, pp. 557–561, University of Alaska Fairbanks, Fairbanks, AK, 2008.
  - Haeberli, W.: Untersuchungen zur Verbreitung von Permafrost zwischen Flüelapass und Piz Grialetsch (Graubünden), vol. 17 of *Mitteilungen der Versuchsanstalt für Wasserbau, Hydrologie und Glaziologie der ETH Zürich*, ETH Zürich, Zurich, 1975.
- Hansson, A., Shulmeister, J., Dargusch, P., and Hill, G.: A review of factors controlling Southern Hemisphere treelines and the implications of climate change on future treeline dynamics, Agricultural and Forest Meteorology, p. 109375, https://doi.org/10.1016/j.agrformet.2023.109375, 2023.
  - Harris, C., Davies, M. C. R., and Etzelmüller, B.: The assessment of potential geotechnical hazards associated with mountain permafrost in a warming global climate, Permafrost and Periglacial Processes, 12, 145–156, https://doi.org/10.1002/ppp.376, 2001.
- Hauck, C.: New concepts in geophysical surveying and data interpretation for permafrost terrain, Permafrost and Periglacial Processes, 24, 131–137, https://doi.org/10.1002/ppp.1774, 2013.
  - Hijmans, R. J.: terra: spatial data analysis, https://rspatial.org/, R package version 1.8-25, https://rspatial.github.io/terra/, 2025.
  - Hilbich, C., Hauck, C., Mollaret, C., Wainstein, P., and Arenson, L. U.: Towards accurate quantification of ice content in permafrost of the Central Andes Part 1: Geophysics-based estimates from three different regions, The Cryosphere, 16, 1845–1872, https://doi.org/10.5194/tc-16-1845-2022, 2022.
  - Hjort, J. and Luoto, M.: Statistical methods for geomorphic distribution modeling, pp. 53–73, Elsevier, https://doi.org/10.1016/B978-0-12-374739-6.00028-2, 2013.





- Hoelzle, M., Mittaz, C., Etzelmüller, B., and Haeberli, W.: Surface energy fluxes and distribution models of permafrost in European mountain areas: An overview of current developments, Permafrost and Periglacial Processes, 12, 53–68, https://doi.org/10.1002/ppp.385, 2001.
- 430 Hosmer, D. W. and Lemeshow, S.: Applied logistic regression, John Wiley & Sons Inc., USA, 2000.
  - Hu, Z., Yan, D., Feng, M., Xu, J., Liang, S., and Sheng, Y.: Enhancing mountainous permafrost mapping by leveraging a rock glacier inventory in northeastern Tibetan Plateau, International Journal of Digital Earth, 17, 2304 077, https://doi.org/10.1080/17538947.2024.2304077, 2024.
- Huggel, C., Fischer, L., Schneider, D., and Haeberli, W.: Research advances on climate-induced slope instability in glacier and permafrost high-mountain environments, Geographica Helvetica, 65, 146–156, https://doi.org/10.5194/gh-65-146-2010, 2010.
  - Janke, J.: Modeling past and future alpine permafrost, Earth Surface Processes and Landforms, 30, 1495–1580, 2005.
  - Jiang, H., Zheng, G., Yi, Y., Chen, D., Zhang, W., Yang, K., and Miller, C. E.: Progress and challenges in studying regional permafrost in the Tibetan Plateau using satellite remote sensing and models, Frontiers in Earth Science, 8, 560 403, https://doi.org/10.3389/feart.2020.560403, 2020.
- Jiang, S., Sweet, L.-b., Blougouras, G., Brenning, A., Li, W., Reichstein, M., Denzler, J., Shangguan, W., Yu, G., Huang, F., et al.: How interpretable machine learning can benefit process understanding in the geosciences, Earth's Future, 12, e2024EF004540, https://doi.org/10.1029/2024EF004540, 2024.
  - Jones, D. B., Harrison, S., Anderson, K., and Whalley, W. B.: Rock glaciers and mountain hydrology: A review, Earth-Science Reviews, 193, 66–90, https://doi.org/10.1016/j.earscirev.2019.04.001, 2019.
- 445 Keller, F.: Automated mapping of mountain permafrost using the program PERMAKART within the geographical information system ARC/INFO, Permafrost and Periglacial Processes, 3, 133–138, 1992.
  - Koenig, C. E. M., Hilbich, C., Hauck, C., Arenson, L. U., and Wainstein, P.: Thermal state of permafrost in the Central Andes (27–34° S), The Cryosphere, 19, 2653–2676, https://doi.org/10.5194/tc-19-2653-2025, 2025.
  - Lewkowicz, A. and Ednie, M.: Probability mapping of mountain permafrost using the BTS method, Wolf Creek, Yukon Territory, Canada, Permafrost and Periglacial Processes, 15, 67–80, https://doi.org/10.1002/ppp.480, 2004.
  - Mahanta, K. K., Pradhan, I. P., Gupta, S. K., and Shukla, D. P.: Assessing machine learning and statistical methods for rock glacier-based permafrost distribution in northern Kargil region, Permafrost and Periglacial Processes, 35, 262–277, https://doi.org/10.1002/ppp.2240, 2024.
- Marcer, M., Bodin, X., Brenning, A., Schoeneich, P., Charvet, R., and Gottardi, F.: Permafrost favorability index: Spatial modeling in the French Alps using a rock glacier inventory, Frontiers in Earth Science, 5, 105, https://doi.org/10.3389/feart.2017.00105, 2017.
  - Masiokas, M. H., Rabatel, A., Rivera, A., Ruiz, L., Pitte, P., Ceballos, J. L., Barcaza, G., Soruco, A., Bown, F., Berthier, E., Dussaillant, I., and MacDonell, S.: A review of the current state and recent changes of the Andean cryosphere, Frontiers in Earth Science, 8, 99, https://doi.org/10.3389/feart.2020.00099, 2020.
- Mollaret, C., Hilbich, C., Pellet, C., Flores-Orozco, A., Delaloye, R., and Hauck, C.: Mountain permafrost degradation documented through a network of permanent electrical resistivity tomography sites, The Cryosphere, 13, 2557–2578, https://doi.org/10.5194/tc-13-2557-2019, 2019.
  - NASA JPL: NASADEM Merged DEM Global 1 arc second V001, https://doi.org/10.5067/MEaSUREs/NASADEM/NASADEM\_HGT.001, accessed 2023-10-30, 2020.
- Popescu, R., Filhol, S., Etzelmüller, B., Vasile, M., Plesoianu, A., Vîrghileanu, M., Onaca, A., Şandric, I., Săvulescu, I., Cruceru, N., Vespremeanu-Stroe, A., Westermann, S., Sîrbu, F., Mihai, B., Nedelea, A., and Gascoin, S.: Permafrost distribution in the



475



- southern Carpathians, Romania, derived from machine learning modeling, Permafrost and Periglacial Processes, 35, 243–261, https://doi.org/10.1002/ppp.2232, 2024.
- Pruessner, L., Phillips, M., Farinotti, D., Hoelzle, M., and Lehning, M.: Near-surface ventilation as a key for modeling the thermal regime of coarse blocky rock glaciers, Permafrost and Periglacial Processes, 29, 152–163, https://doi.org/10.1002/ppp.1978, 2018.
- 470 Pya, N.: Package 'scam': Shape constrained additive models, R package, 2023.
  - Pya, N. and Wood, S. N.: Shape constrained additive models, Statistics and Computing, 25, 543–559, https://doi.org/10.1007/s11222-013-9448-7, 2015.
  - RGIK Working Group: Guidelines for inventorying rock glaciers: Baseline and practical concepts (version 1.0), Tech. rep., IPA Action Group Rock Glacier Inventories and Kinematics, Université de Fribourg, https://roar.hep-bejune.ch/documents/327247/files/231228\_RoGI BPCv1.0.pdf, 2023.
  - Roer, I. and Nyenhuis, M.: Rockglacier activity studies on a regional scale: Comparison of geomorphological mapping and photogrammetric monitoring, Earth Surface Processes and Landforms, 32, 1747–1758, https://doi.org/10.1002/esp.1496, 2007.
  - Rouyet, L., Delaloye, R., Bertone, N., Marcer, M., and et al.: Rock glacier inventories (RoGIs) in 12 areas worldwide using a multi-operator consensus-based procedure, Earth System Science Data, 17, 4125–4150, https://doi.org/10.5194/essd-17-4125-2025, 2025.
- 480 Saito, K., Trombotto, D., Yoshikawa, K., Mori, J., Sone, T., Marchenko, S., Romanovsky, V., Walsh, J., Hendricks, A., and Bottegal, E.: Late quaternary permafrost distribution downscaled for South America: Examinations of GCM-based maps with observations, Permafrost and Periglacial Processes, 27, 43–55, https://doi.org/10.1002/ppp.1863, 2015.
  - Sattler, K., Anderson, B., Mackintosh, A., Norton, K., and de Róiste, M.: Estimating permafrost distribution in the maritime Southern Alps, New Zealand, based on climatic conditions at rock glacier sites, Frontiers in Earth Science, 4, https://doi.org/10.3389/feart.2016.00004, 2016.
  - Selley, H., Harrison, S., Glasser, N., Wündrich, O., Colson, D., and Hubbard, A.: Rock glaciers in central Patagonia, Geografiska Annaler: Series A, Physical Geography, 101, 1–15, https://doi.org/10.1080/04353676.2018.1525683, 2018.
  - Senate of Chile: Boletin 11876-12, https://tramitacion.senado.cl/appsenado/templates/tramitacion/index.php?boletin\_ini=11876-12, 2023.
- Wicky, J. and Hauck, C.: Air convection in the active layer of rock glaciers, Frontiers in Earth Science, 8, 335, https://doi.org/10.3389/feart.2020.00335, 2020.
  - Wood, S. N.: Generalized Additive Models: An Introduction with R, CRC Press, 2nd edn., 2017.
  - Yoshikawa, K., Casassa, G., Azócar, G., Iribarren Anacona, P., Masías, P., Miyata, T., and Cáceres Correa, B.: Permafrost and active layer characteristics in the high arid Andes between the Altiplano and high Atacama Desert, Arctic, Antarctic, and Alpine Research, 57, https://doi.org/10.1080/15230430.2025.2532202, 2025.